ACI MATERIALS JOURNAL TECHNICAL PAPER

Title no. 99-M47

# Interface Tailoring for Strain-Hardening Polyvinyl Alcohol-Engineered Cementitious Composite (PVA-ECC)

by Victor C. Li, Cynthia Wu, Shuxin Wang, Atsuhisa Ogawa, and Tadashi Saito

*Polyvinyl alcohol (PVA) fiber tends to rupture instead of pullout in a cementitious matrix due to the strong chemical bonding to cement hydrates and the slip-hardening response during pullout. In order to achieve strain-hardening behavior at the composite level, the micromechanical models suggest that the bond should be lowered to an optimal range. Following this quantitative guidance, the interface is engineered by applying oil coating to the fiber surface. The experimental study confirms the effectiveness of this approach. With an appropriate oiling agent amount, PVA fiber-reinforced Engineered Cementitious Composites (ECC) with tensile strain capacity exceeding 4% and with saturated multiple cracking are demonstrated.*

**Keywords:** chemical bond; slip; strain.

## INTRODUCTION

Many infrastructure deterioration problems and failures can be traced back to the cracking and brittle nature of concrete. It is no wonder that significant research efforts have gone into attempts at enhancing the ductility of concrete materials. To date, the most effective means of imparting ductility into concrete is by means of fiber reinforcement. Most fiber-reinforced concrete results in enhanced postpeak tension-softening behavior under tensile load. This improved toughness is useful in resisting the propagation of cracks into major fractures by energy absorption in the bridging actions of fibers in the fracture process zone.[1]

While the fracture toughness of concrete can increase by an order of magnitude by fiber reinforcement, the tensile strain capacity usually remains little changed. In recent years, efforts to convert this quasibrittle behavior of fiber-reinforced concrete (FRC) to ductile strain-hardening behavior resembling ductile metal have met with varying degrees of success. In most instances, the approach is to increase the fiber content as much as possible, and processing techniques are adapted to overcome the resulting workability problem. Cement-based composites such as slurry infiltrated fiber concrete (SIFCON) and slurry infiltrated mat concrete (SIMCON) are good examples of this approach, which utilizes from 5 to 20% volume content of steel fibers. The drawback of such an approach is that the range of suitable applications is limited by the special processing needs. Also, high-fiber content leads to high material cost that further restricts the practical applications of such materials.

Starting with the classical work of Aveston, Cooper, and Kelly on the micromechanics of strain-hardening in cement composites reinforced with aligned continuous fiber,[2] the last decade has seen rapid development of understanding in the micromechanics of strain-hardening in cementitious composites reinforced with short randomly distributed fibers.[3,4] The new knowledge has provided an excellent foundation for the design of strain-hardening cementitious composites (engineered cementitious composite, or ECC) with tensile strain capacity in excess of 3%. In comparison, materials like SIFCON and SIMCON typically have tensile strain capacities of less than 1.5% when measured by uniaxial tension tests using dog-bone-shaped specimens with a cross section of 76 x 38 mm (fiber length 30 mm).[5] The tensile strain capacity of a commercial fiber-reinforced cementitious composite known as DUCTAL has a tensile strain capacity of less than 0.5%.[6]

Li reported an ECC reinforced with 2% ultra-high molecular weight polyethylene fibers having a tensile strain capacity of 6 to 8%.[7] Using very large-sized "compact" tension specimens (585 x 490 x 35 mm), the fracture toughness of this material was determined to be more than 35 kJ/m$^2$, approaching that of aluminum alloys.[8,9] Significant damage tolerance of this PE-ECC was demonstrated using a series of uniaxial tension specimens with different notch lengths.[10] Maalej and Li illustrated the application of such ductile materials in the form of a concrete cover in a reinforced concrete (R/C) beam.[11] Under 4-point loading, the standard R/C beam experienced a crack width in the concrete cover of 1.6 mm at peak load, while the R/C beam with the PE-ECC cover experienced a crack width of 0.2 mm at a similar load level. This test result suggests the potential use of materials like ECC in enhancing structural durability. ECC is being investigated for use in earthquake-resistant structures.[12-14]

Practical applications of ECC, however, are limited by the high cost of ultra-high molecular weight polyethylene fibers. In search of a replacement, polyvinyl alcohol (PVA) fiber has emerged as the most promising alternative. Other low-cost fibers, such as Nylon, low-density polyethylene fiber, and polypropylene fiber, are less suitable due to low tensile strength and low modulus of elasticity. A number of attempts at applying off-the-shelf PVA fiber, however, have resulted in composites with significantly lower tensile strain capacities on the order of 0.5 to 1.0% even if as much as 4% fiber volume fraction is used.[15,16] The present paper describes a systematic approach at developing a PVA-ECC with a tensile strain capacity of 4 to 5%. The special PVA fiber used is a result of applying micromechanical models to tailor the fiber geometric and mechanical properties conducted at the University of Michigan and the fiber spinning and heat treatment technology developed at Kuraray Corp. Development of a ductile composite requires tailoring the fiber, matrix, and interface. Information on fiber tailoring can be

*ACI Materials Journal*, V. 99, No. 5, September-October 2002.
MS No. 01-334 received October 5, 2001, and reviewed under Institute publication policies.  Pertinent discussion will be published in the July-August 2003 *ACI Materials Journal* if received by April 1, 2003.

*ACI member* **Victor C. Li** *is a professor of Civil and Environmental Engineering at the University of Michigan, Ann Arbor, Mich. His research interests include micromechanics-based composite materials design and engineering, innovative structures design based on advanced materials technology, and infrastructure engineering.*

**Cynthia Wu** *received her PhD in 2001 from the Department of Civil and Environmental Engineering at the University of Michigan. Her research interests include tailoring of fibers and fiber/matrix interface for ductile composite design.*

**Shuxin Wang** *is a graduate student research assistant in the Department of Civil and Environmental Engineering at the University of Michigan. He received his BS and MS from Tsinghua University in Beijing. His research interests include the development of engineered cementitious composite and application of fiber-reinforced plastic reinforcement.*

**Atsuhisa Ogawa** *is an employee of the ECC/FRC R&D group, Kuraray Company, Osaka, Japan.*

**Tadashi Saito** *is a research and development engineer of fiber-reinforced concrete, Kuraray Company.*

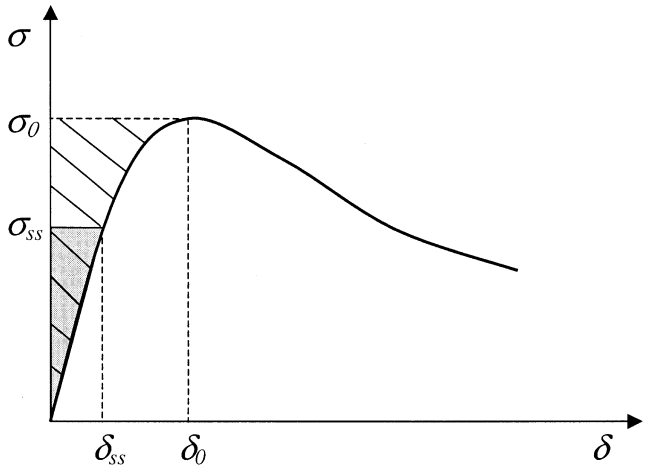


*Fig. 1—Typical s(d) curve for strain-hardening material. (Shaded area represents right-hand side of Eq. (1); hatched area represents maximum complementary energy* $J_b'$ *of composite.)*

found in Wu.[17] An initial study on matrix tailoring using fine sand was reported in Li, Wang, and Wu.[18] In this paper, focus is placed on the tailoring of the fiber/matrix interface to create the extremely ductile PVA-ECC composite.

The challenge of using PVA fibers in cementitious matrix reinforcement is that PVA fibers tend to develop very strong chemical bonding with cement due to the presence of the hydroxyl group in its molecular chains. This high chemical bonding leads to a tendency of fiber rupture and limits the tensile strain capacity of the resulting composite.[16] Furthermore, Redon et al.[19] observed a strong slip-hardening response during fiber pullout that can lead to a shear-delamination failure of the PVA fiber. The objective of interface tailoring for PVA fibers is to control the interface bond and the slip-hardening behavior. In this paper, a fiber coating in the form of an oiling agent is adopted as the means of interface properties control.

In the following, the micromechanics theoretical basis of interface tailoring is first reviewed. The interface properties test and composite properties test, as well as the materials used in the experimental program, are then summarized. Results on the influence of different oiling content on the interface properties and composite properties are then reported and discussed. Conclusions are drawn on the effectiveness of this micromechanics-based interface tailoring approach for tensile strain-hardening of PVA-ECC.

## RESEARCH SIGNIFICANCE

This paper presents the development of the PVA-ECC in the context of material design under the guidance of micromechanical tools. Specifically, this study illustrates how the fiber/matrix interface may be engineered to accommodate the requirements imposed by the micromechanical models thus highlighting the importance of interface tailoring on the composite performance. This micromechanics-based material design approach is broadly applicable to achieving high-performance composites with low fiber content for cost-effective structural applications.

## THEORETICAL GUIDELINES FOR INTERFACE TAILORING

The micromechanics of tensile strain-hardening for cementitious composites reinforced with randomly oriented short fibers have been extensively studied. These studies focus on two aspects: the requirement of bridging properties of fibers in the form of stress-crack opening $\sigma$–$\delta$ relationship, or simply $\sigma(\delta)$ for steady-state crack propagation[20, 21] necessary for composite strain-hardening behavior, and the influence of interface and fiber properties on the $\sigma$–$\delta$ relationship.[3] When combined, these analyses lead to guidelines for the tailoring of fiber, matrix, and interface to attain strain-hardening with the minimum amount of fibers.[7] In this section, the requirements on interface properties of PVA fibers for creating strain-hardening PVA-ECC is highlighted. This serves as the theoretical background for the experimental investigation on interface and composite characterization studies to be presented in the following.

Steady-state crack propagation means that a crack increases in length at constant ambient tensile stress $\sigma_{ss}$ while maintaining a constant crack opening $\delta_{ss}$ (a flat crack, with the exception of a small region near the crack tip). Marshall and Cox showed that this phenomenon prevails (over that of the typical Griffith type crack) when the condition[1]

$$J_{tip} = \sigma_{ss}\delta_{ss} - \int_0^{\delta_{ss}} \sigma(\delta)d\delta \qquad (1)$$

is satisfied. In Eq. (1), $J_{tip}$ approaches the matrix toughness $K_m^2/E_m$ at small fiber content, appropriate for ECC because less than 3% fiber by volume is used. (The matrix fracture toughness $K_m$ and Young's Modulus $E_m$ are sensitive to the details of mixture design, such as water-cementitious material ratio [*w/c*] and sand size and content.) The right-hand side of Eq. (1) may be interpreted as the energy supplied by external work less that dissipated by the deformation of the "inelastic springs" at the crack tip process zone opening from 0 to $\delta_{ss}$. The inelastic springs concept is a convenient means of capturing the inelastic processes of fiber deformation/breakage and interface debonding/slippage of those fibers bridging across the crack faces in the process zone. Hence, Eq. (1) expresses the energy balance (energy demanded and supplied to crack tip) per unit crack advance during steady-state crack propagation.

Figure 1 schematically illustrates this energy balance concept on a $\sigma(\delta)$ plot. The right-hand side of Eq. (1) is shown as the dark shaded area and is often referred to as the complementary

energy. Since the maximum value (light shaded area) of this complementary energy $J_b'$ occurs when the shaded area extends to the peak stress $\sigma_0$ and crack opening $\delta_0$, it implies an upper limit on the matrix toughness for steady-state crack propagation mode:

$$\frac{K_m^2}{E_m} \le \sigma_o \delta_o - \int_0^{\delta_o} \sigma(\delta) d\delta \equiv J_b' \quad (2)$$

It is clear from Eq. (2) that the successful design of an ECC requires the tailoring of matrix, fiber, and interface properties. Specifically, the fiber and interface properties control the shape of the $\sigma(\delta)$ curve and are therefore the dominant factors governing $J_b'$. The composite design for strain-hardening requires the tailoring of the fiber/matrix interface to maximize the value of $J_b'$. This paper examines the effectiveness of achieving high ductility via high values of $J_b'$ by surface coating of PVA fiber using an oiling agent.

The shape of the $\sigma(\delta)$ curve and especially the rising branch associated with $J_b'$ shown in Fig. 1 is related to a number of fiber/matrix interaction mechanisms. In the simplest case when fibers and matrix are in frictional contact only, the slope of the rising branch of the $\sigma(\delta)$ curve, or the stiffness of the bridges, is mainly governed by the fiber content $V_f$, the fiber diameter $d_f$, fiber length $L_f$ and stiffness $E_f$, and the interface frictional bond $\tau_0$. In the case when chemical bond $G_d$ is present, the starting point of the $\sigma(\delta)$ is not at the origin of the plot but is shifted upwards. This reflects the need of a certain amount of load on the fibers and interface before the interfacial chemical bond can be broken. Dedonding is needed to allow for deformation of the debonded fiber segment to produce crack opening $\delta$. Thus, the presence of $G_d$ typically diminishes the complementary energy $J_b'$.

The peak value of the $\sigma(\delta)$ curve is mainly governed by $V_f$, $d_f$, $L_f$, $\tau_0$ in the case of simple friction pullout. An analytic expression of $\sigma_0$ can be found in Li.[21] In the presence of $G_d$, the higher load on the fiber can lead to fiber rupture. Thus, for given fiber strength $\sigma_f$, the complementary energy $J_b'$ again decreases with $G_d$.

The above discussions suggest that high $G_d$ value can invalidate the inequality expressed in Eq. (2) for strain-hardening. Figure 2(a) confirms this negative influence of $G_d$ on $\sigma(\delta)$ curves computed using the micromechanical model of Lin, Kanda, and Li.[22] This micromechanical model accounts for the mechanical interactions between fiber and matrix at the interface and is due to inclined fiber bridging, as well as the random distribution nature of fiber location (relative to the crack plane) and orientation. Most importantly, the tendency of fiber rupture as the crack opens is included in the model. An almost linear decay of $J_b'$ with increasing $G_d$ is found (Wu 2001, Fig. 2(b)). A 54% drop in $J_b'$ is observed when $G_d$ increases from 1 to 5 J/m$^2$. Because of the presence of the hydroxyl (OH) group in PVA, the chemical bond is high. A single-fiber pullout test by Lin, Kanda, and Li. indicated a typical value in the range of 3 to 5 J/m$^2$. In comparison, the commonly used polypropylene (PP) fiber typically has no chemical bond ($G_d = 0$) in a cementitious matrix.

Redon, Li, and Wu discovered that rupture of PVA fiber is still possible even after the fiber has completely debonded.[19] Typical single PVA fiber pullout curves are shown in Fig. 3. The breaking of the chemical bond is clearly reflected in the first load drop. Subsequently, the load increases again with

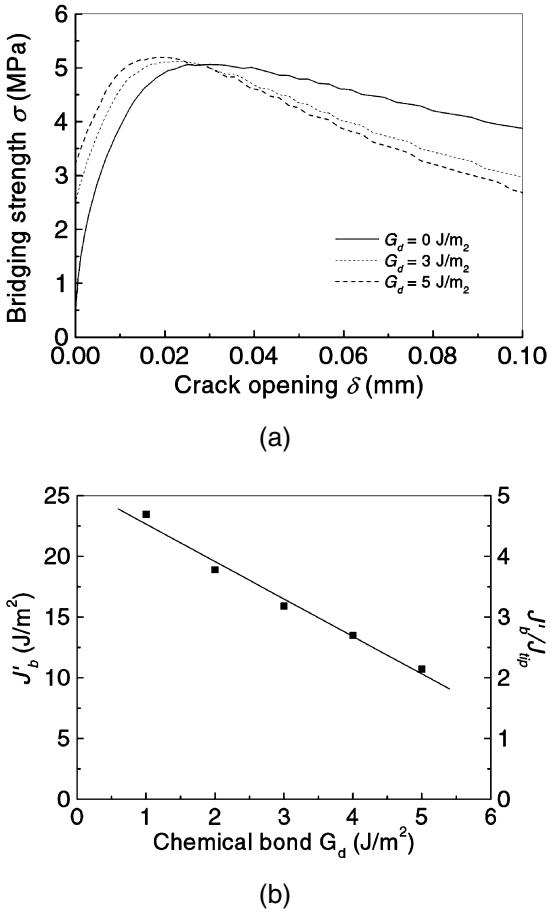


*Fig. 2—(a) Effect of interfacial fracture toughness* $G_d$ *on computed* $\sigma(\delta)$ *curve; and (b) effect of* $G_d$ *on computed complementary energy* $J_b'$ *and pseudo strain hardening (PSH) index* $J_b'/J_{tip}$,[25] *where* $J_{tip} = 5$ *J/m*$^2$ *is assumed.*

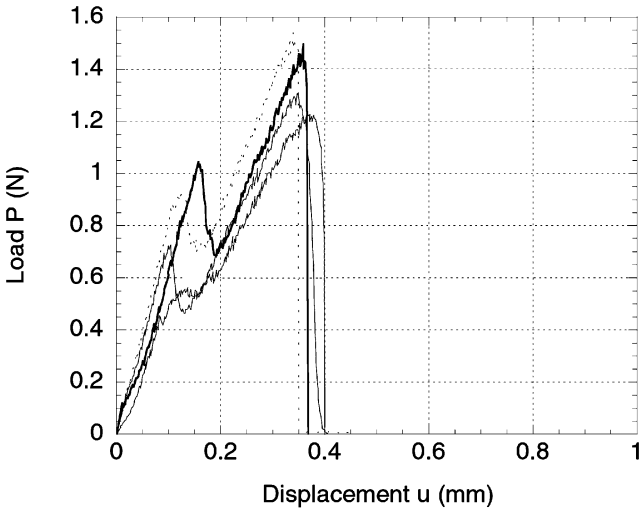


*Fig. 3—Typical pullout behavior of PVA fiber from cementitious matrix. Fiber embedded lengths are 0.56 to 0.71 mm. Incomplete pullout occurs due to fiber rupture during slip-hardening.*

fiber pullout. This increase is interrupted by a final sudden load-drop. On examining the pullout segment, the fiber is found to be severely damaged, often resulting in a pencil-sharpened shape of the fiber end. The slip-hardening process,

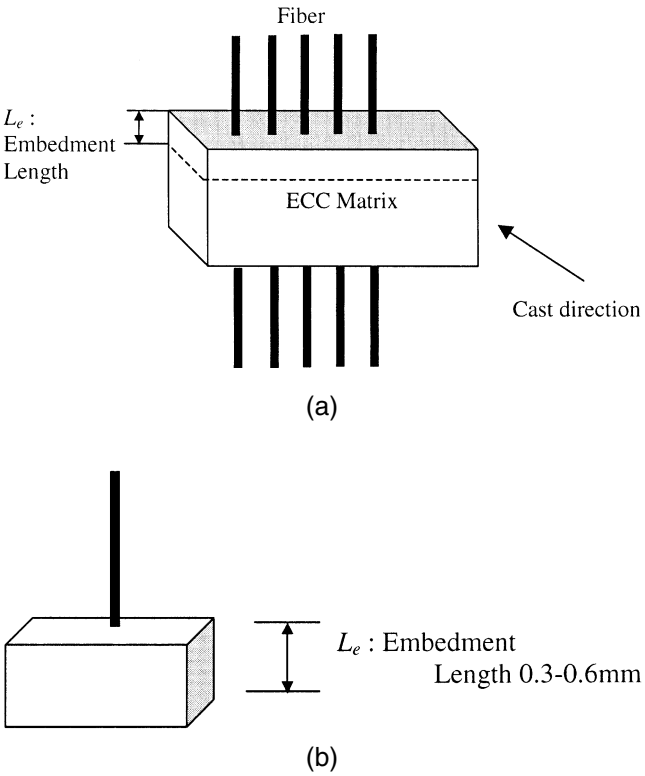


*Fig. 4—Pullout specimen configuration: (a) Cast specimen with multiple fibers; and (b) cut specimen with single fiber.*

associated with surface fibrillation and jamming of the fiber, is beneficial to enhancing $J_b'$. Excessive slip-hardening, however, can lead to premature fiber rupture and reduction in $J_b'$.

A complete analytic model of the $\sigma(\delta)$ curve that includes both chemical bond $G_d$ and slip-hardening coefficient $\beta$ can be found in Lin, Kanda, and Li.[22] This model was used by Wu[17] to determine targets of interface property tailoring. She found that for the PVA fiber described in the section Experimental Program, the optimal ranges of interfacial properties are: $G_d < 2.2$ J/m$^2$; $\tau_0 = 1.0 - 2.1$ MPa; and $\beta < 1.5$. These parametric values were calculated based on an assumed value of $J_{tip} = 5$ J/m$^2$, typical for the type of cementitious matrix used in this study.

## EXPERIMENTAL PROGRAM

Two sets of experiments are conducted to investigate the effectiveness of interface tailoring: single-fiber pullout test at interface level and uniaxial tension test at composite level. The major parameter investigated here is the effect of the oiling agent amount on the interfacial bond properties. From the single-fiber pullout test, the bond properties including $\tau_0$, $G_d$, and $\beta$ can be quantified.[19] The amount of oiling agent can then be adjusted to tailor the bond properties to the optimal ranges previously described. A uniaxial tension test, which characterizes the strain-hardening behavior, is then conducted to verify the micromechanics model prediction.

### Materials

The specific PVA fiber used in the present study has mechanical and geometrical properties described in Table 1. For the single-fiber pullout test, continuous fiber is used. The apparent strength denotes the reduced fiber strength when the fiber is embedded in cementitious matrix. The fibers are coated with various amounts of a proprietary oiling agent that reduces the hydrophilicity of the fiber surface. Five levels of coating are applied: 0, 0.3, 0.5, 0.8, and 1.2%. These percentages represent the ratio of the weight of oil coating to the weight of the fiber. According to the manufacturer, the thickness of the applied coating layer is about 100 nm and has strong adhesion to the fiber surface; therefore, the loss of oil coating during mixing is expected to be small.

**Table 1—Properties of PVA fiber**

| Nominal strength, MPa | Apparent strength, MPa | Diameter, μm | Length, mm | Young's modulus, GPa | Elongation, % |
|---|---|---|---|---|---|
| 1620 | 1092 | 39 | 12 | 42.8 | 6.0 |

**Table 2—Matrix composition**

| *w/c* | *s/c* | SP, % | Viscosity agent | Defoamer, % |
|---|---|---|---|---|
| 0.45 | 0.6 | 2.0 | 0.15 | 0.05 |

The main components of the dry mixture consist of Type I portland cement, along with fine sand (F110, 50 to 150 μm). The chemical additives used are a dry viscosity agent (methyl cellulose), a dry defoamer that reduces the air bubbles generated by the viscosity agent, and a high-range water-reducing admixture to adjust the workability. The complete matrix composition, which is used in both the interface test and composite test, is shown in Table 2. The fiber volume fraction in composite is 2%.

### Specimen configuration and preparation—interface test

The specimen configuration and dimensions are shown in Fig. 4. The specimens were prepared using a technique described in detail in Reference 23. Continuous fibers were taped to a plastic mold for alignment control. The matrix was prepared and poured into the mold. Vibration was applied for less than 2 min. A plexiglass plate was then placed over the rectangular specimen to compact the material, and a wet cloth was placed over the plate. This is to ensure a moist environment and to avoid shrinkage cracks from forming. The specimens were demolded after 48 h to secure a hardened state. After demolding, the specimens were wrapped in wet cloths until testing. Fifty to 60% humidity was maintained and the wet cloths were periodically moistened to avoid drying. After 21 days, the specimens were tested. The day before testing, the specimens were cut with a diamond saw under running water to the desired thickness, which was also the fiber embedment length. The specimens were then laid out to dry for 1 day. The curing conditions were chosen to simulate that of the composite tests, where the specimens were wet cured and then dried for 1 day before testing.

### Specimen configuration and preparation—composite test

The specimen measured 304.8 x 76.2 x 12.7 mm (L x W x H) in the shape of a rectangular coupon. The gage length of the specimen was approximately 185 mm. Typically three or four specimens were tested for each material composition.

In a small mixer with a planetary rotating blade, the cement, sand, and defoamer were dry mixed for approximately 1 to 2 min at low speed. During this time, the methyl cellulose

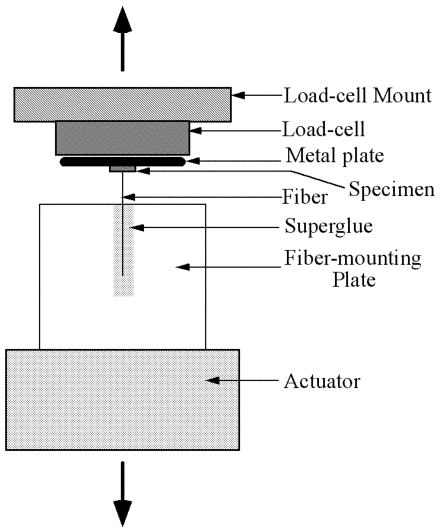


*Fig. 5—Test setup of single fiber pullout test.*

was fully dissolved in a portion of the measured water to form a liquid solution. After the dry contents were fully mixed, the remaining water was added and mixed for another 2 min at low speed. Shortly after, the methyl cellulose solution was added and mixed for approximately 10 min to completely activate the absorption of the methyl cellulose onto the cementitious particles. Then the high-range water-reducing admixture was added and mixed at a higher speed for approximately 1 to 2 min. Finally, the fibers were manually added in small amounts until all fibers were dispersed into the cementitious matrix.

After the mixture was completed, the material was poured into greased plexiglass molds. The specimens were then vibrated for approximately 3 to 4 min while the specimen surface was smoothed over with a spatula. The smoothness of the specimen surface was important to prevent failure at the grips since aluminum plates for tension gripping would be glued onto both sides at each end of the specimen. In addition, large air bubbles can be entrapped underneath the paper towels placed over the surface after casting. Variability in air bubbles can alter the crack pattern because flaw size distribution governs the first crack strength and the matrix cracking thereafter. After casting, the specimens were hardened for 24 h and then demolded. The specimens were then cured in a water tank at room temperature for approximately 14 days. It had been found that after 7 days, the tensile properties of ECC composites did not change much; therefore, 14 days curing was chosen for testing.[24] One day before testing, the specimens were taken out of the water tank to glue onto the aluminum plates.

### Single-fiber pullout test setup

The pullout tests were conducted on a load frame with the specimen configuration shown in Fig 5. A 10 N load cell was used with 1.97 N range to measure the pullout load of the fibers with a displacement rate of 0.02 mm/s. The displacement shown on the pullout curve in Fig. 3 was measured as the actuator (± 10 mm stroke) movement. Fiber-free length was kept at a maximum of 1 mm. The displacement pertaining to peak debonding load $P_a$ was approximately 0.1 mm. This value was subtracted from the slippage distance for the calculation of $\beta$. The bottom of the specimen was glued onto the metal plate that was screwed into the small load cell. The fiber-free

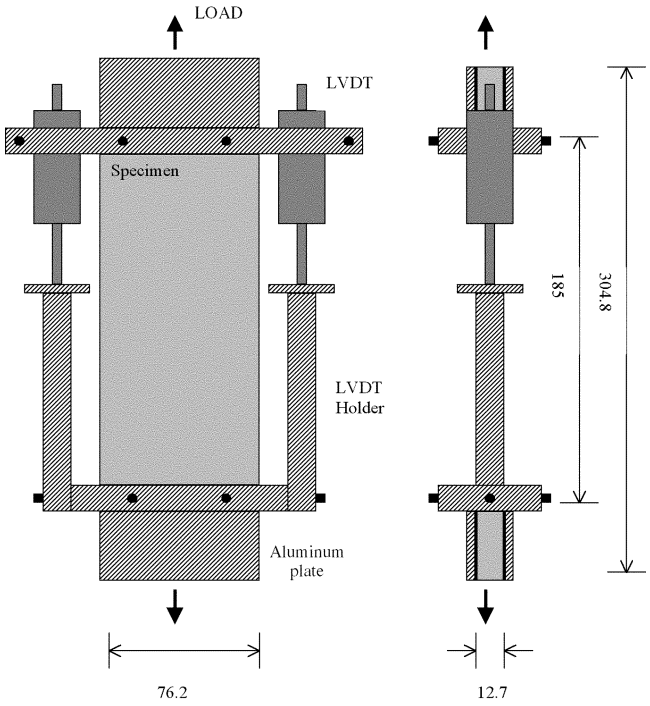


*Fig. 6—Test setup for uniaxial tensile test (note: all dimensions in mm).*

end was then glued to an aluminum plate and then secured with tape. A microscope was used to ensure that the fiber was properly aligned normal to the matrix.

### Uniaxial tension test setup

Tensile coupon specimens were tested in a load frame with a 25 kN capacity with fixed hydraulic grips. The displacement rate used was 0.0025 mm $s^{-1}$ throughout the test for both elastic and inelastic portions of the tensile response. The test setup is shown in Fig. 6. Two linear variable displacement transducers (LVDTs) were placed on each side of a specimen to measure the uniaxial strain with an approximate gage length of 185 mm. Aluminum plates were glued (with epoxy) on both ends for adequate gripping conditions. Special attention was given to ensure proper alignment of the specimens with the hydraulic grips. The load frame machine works in conjunction with computer software for data collection. The load and actuator displacement data were recorded. Crack openings were measured with an optical microscope with a video output utilizing a 200X magnification after testing, where the width of the final failure crack was not counted. The experimental crack spacing was measured by counting the number of cracks under the microscope within a constant specified length. In this case, a constant length of 150 mm in the middle of the specimen was used. Typically, this procedure involved more than 60 cracks for a multiple-crack saturated specimen. The length was then divided by the number of cracks to determine the crack spacing $x_d$.

## EXPERIMENTAL RESULTS

### Oiling effect on interface properties

Figure 7(a) to (c) show the effect of oiling quantity on $\tau_0$, $G_d$, and $\beta$. Complete data on these interface properties are tabulated in Table 3. The model and method of extracting these parameters from single-fiber pullout curves have been documented in detail in Reference 22. The targeted

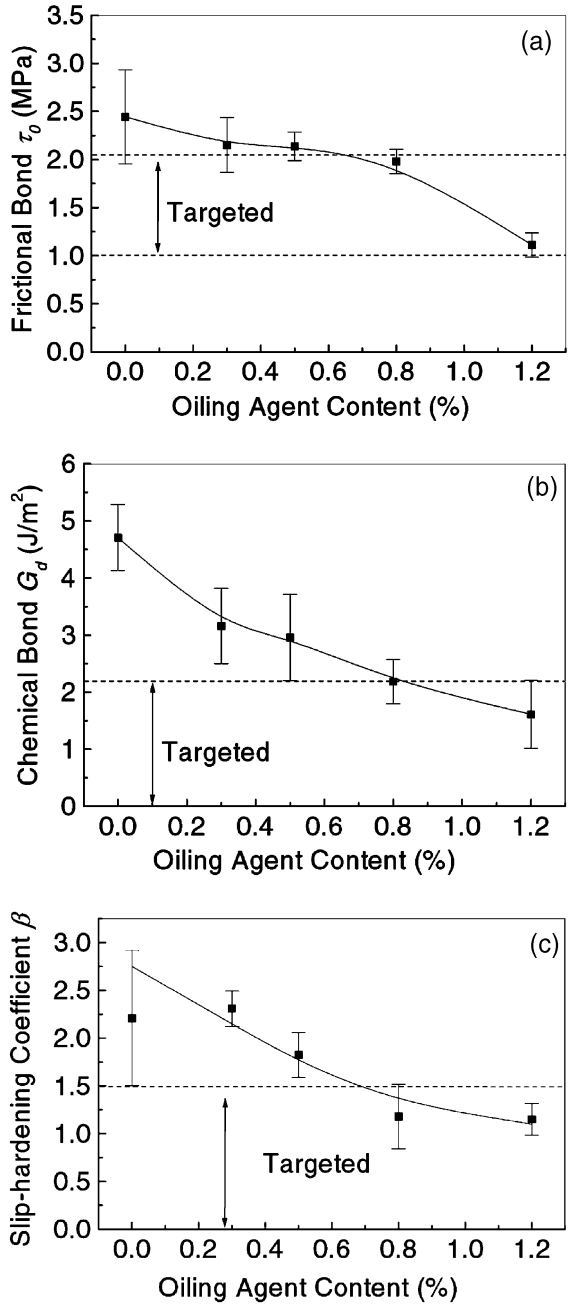


*Fig. 7—Effect of oiling content on interfacial properties.*

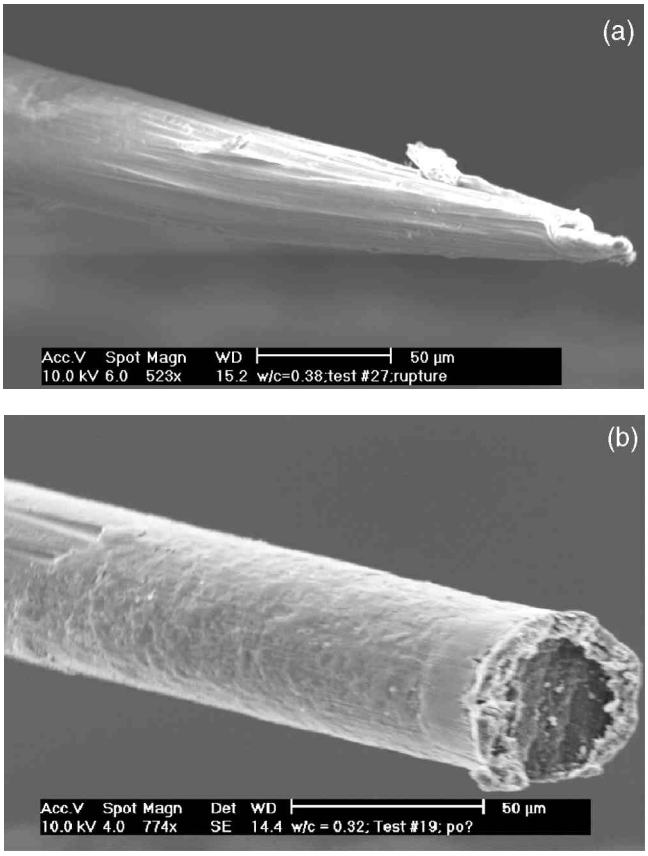


*Fig. 8—Effect of oiling agent on delamination of PVA fiber: (a) Ruptured end of non-oiled fiber; and (b) pulled out end of oiled fiber.*

**Table 3—Effect of oiling on interfacial properties and micromechanical predictions of complementary energy $J_b'$***

| Oiling quantity, % | $\tau_0$, MPa | $G_d$, J/m$^2$ | $\beta$ | $J_b'$, J/m$^2$ | $J_b'/J_{tip}$ |
|---|---|---|---|---|---|
| 0.0 | 2.44 ± 0.49 | 4.71 ± 0.58 | 2.21 ± 0.71 | 3.64 – 6.63 | 0.73 – 1.33 |
| 0.3 | 2.15 ± 0.19 | 3.16 ± 0.66 | 2.31 ± 0.19 | 5.17 – 13.8 | 1.03 – 2.76 |
| 0.5 | 2.14 ± 0.15 | 2.96 ± 0.75 | 1.82 ± 0.23 | 7.68 – 13.6 | 1.54 – 2.72 |
| 0.8 | 1.98 ± 0.13 | 2.18 ± 0.39 | 1.18 ± 0.34 | 12.5 – 20.7 | 2.50 – 4.14 |
| 1.2 | 1.11 ± 0.13 | 1.61 ± 0.60 | 1.15 ± 0.17 | 24.2 – 38.1 | 4.84 – 7.62 |

*$J_{tip}$ ~ 5 J/m$^2$ assumed for $J_b'/J_{tip}$ calculations.

ranges indicated in Fig. 7 are the optimal ranges mentioned in the earlier section on Theoretical Guidelines for Interface Tailoring.

The general trend is that the interfacial bond properties significantly decrease with the increase of oiling quantity. For example, the average $\tau_0$ is reduced from 2.44 MPa for a nontreated fiber to 1.11 MPa for a 1.2% oiled fiber. The drop of the chemical bond $G_d$ is more dramatic. For nontreated fibers, the average chemical bond $G_d$ is 4.71 J/m$^2$, which drops to 1.61 J/m$^2$ at 1.2% oiling content. The oiling agent also reduces the slip-hardening effects. The slip-hardening coefficient $\beta$ for non-oiled fibers reaches as high as 2.9. This drops to about 1.2 for 1.2% oiled fibers.

The influence of oiling on the pullout behavior of the fiber can be appreciated by comparing Fig. 8(a) and (b). Figure 8(a) shows the ruptured end of a non-oiled PVA fiber, which shows severe delamination failure. When 0.8% oiling is applied, the delamination effect almost completely disappeared, allowing the full embedment length to slide out with little damage. The possible scenario of the delamination process is illustrated schematically in Fig. 9. Figure 9(a) shows the progressive damage of the fiber as it is pulled out from the matrix. The delamination shaves the fiber into a sharp tip towards the deep embedment end because this end travels the most distance in contact with the matrix material prior to exiting the matrix. The four stages of fiber damage illustrated in Fig. 9(a) correspond to the four loading stages in Fig. 9(b), which represents a typical single-fiber pullout curve. Shortly after Stage 3, the fiber completely loses contact with the matrix, with a sudden load drop and a pullout segment $l_{po}$ less than the original embedment length $l_e$.

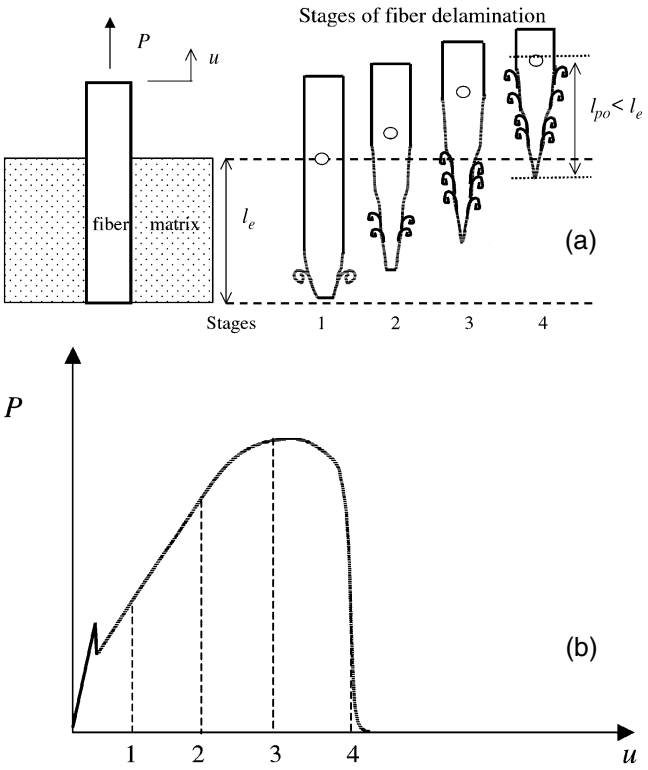


*Fig. 9—(a) Fiber delamination during slip-hardening; and (b) at various stages of pullout process illustrated on* P-u *curve.*

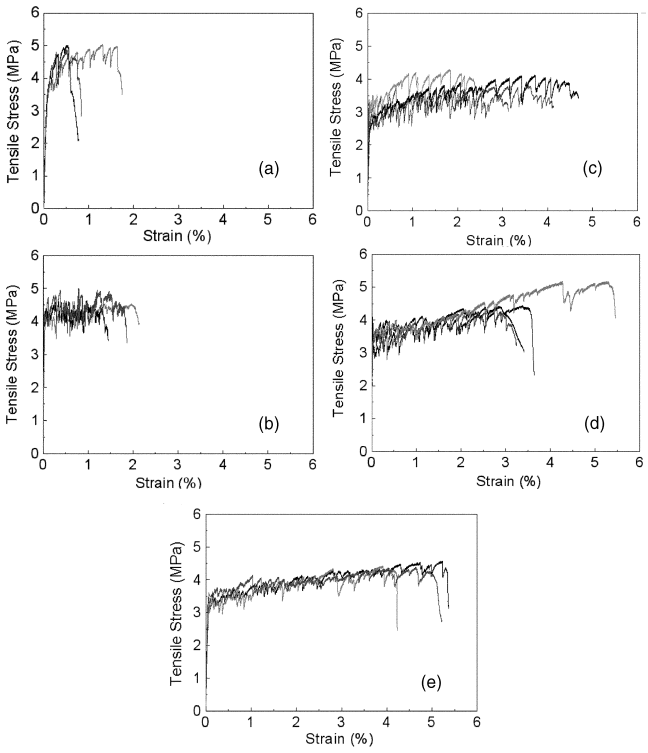


*Fig. 10—Effect of oiling agent content on tensile stress-strain curve of composites with: (a) 0%; (b) 0.3%; (c) 0.5%; (d) 0.8%; and (e) 1.2% oiling content.*

### Oiling effect on composite properties

The stress-strain curves and the corresponding crack patterns of all five sets of specimens with 0, 0.3, 0.5, 0.8, and 1.2% oiling content are shown in Fig. 10 to 12 and Table 4. Because the specimen thickness 12.7 mm is at the same order of fiber length 12 mm, fiber orientation is expected to slightly cluster to the plane normal to thickness direction, although a fiber dispersion very close to 3D random distribution is expected to be a reasonable assumption. Nonetheless, interpretation of the presented strain capacity should be restricted to the specimen configuration adopted in this test.

The nontreated fiber composites barely exhibit multiple cracking behaviors, with an averaged strain capacity below 1%. Few cracks are observed (Fig. 11(a)), and the crack spacing ranges from 15 to approximately 40 mm.

The 0.3% oiled fiber composites show a marginally improved tensile strain capacity of 1.6 ± 0.33%. The crack pattern (Figure 11(b)) shows relatively uneven crack spacing, reflecting unsaturated multiple cracking. The averaged crack spacing is 8 mm.

For the 0.5% oiled fiber composites, the average tensile strain capacity increases to 2.7 ± 0.8%. The higher strain capacity is accompanied by an increase in the number of multiple cracks and a larger crack opening of 52 μm. One of the composites reaches a strain level of 3.8%, indicating that material variation is an important factor in attaining strain-hardening behavior for this fiber. The average crack spacing for this set of specimens is 4 mm. The crack pattern of a 0.5% oiled fiber composite is shown in Fig. 11(c). This particular specimen has a strain capacity of 2.8%.

For the 0.8% oiled fiber composites, the strain capacity achieves an average value of 3.8 ± 1.1%. One of the specimens reached a strain level exceeding 5%, of which the crack pattern approaches full saturation (Fig. 11(d)), and the average crack spacing is approximately 2.5 mm.

Further increase of the oiling agent to 1.2% improves the consistency of the composite behavior, leading to an average strain of 4.88%. The increase in strain capacity is mainly contributed by the wider crack opening, which reaches an average value of 88 μm because the crack spacing does not show further reduction when compared with the 0.8% oiled composites.

**Table 4—Effect of oiling agent content on experimentally measured tensile properties**

| Oiling quantity, % | First crack strength $\sigma_{fc}$, MPa | First tensile strength $\sigma_{cu}$, MPa | Strain capacity $\varepsilon_{cu}$, % | Crack opening $x_d$, mm | Crack opening, μm |
|---|---|---|---|---|---|
| 0.0 | 3.11 ± 0.23 | 4.89 ± 0.07 | 0.99 ± 0.57 | 27.00 ± 12.00 | 43 ± 20 |
| 0.3 | 2.63 ± 0.43 | 4.72 ± 0.17 | 1.55 ± 0.33 | 7.50 ± 2.80 | 44 ± 7 |
| 0.5 | 2.35 ± 0.21 | 4.09 ± 0.22 | 2.73 ± 0.78 | 3.50 ± 1.10 | 52 ± 10 |
| 0.8 | 2.90 ± 0.10 | 4.62 ± 0.36 | 3.81 ± 1.14 | 2.50 ± 0.33 | 71 ± 9 |
| 1.2 | 2.92 ± 0.06 | 4.41 ± 0.15 | 4.88 ± 0.59 | 2.80 ± 0.52 | 88 ± 12 |

## DISCUSSIONS

From the composite test results, it is evident that increasing the oiling agent (at least within the range of this experimental investigation) leads to an increase in tensile strain capacity, accompanied by a larger crack width and reduced crack spacing. The strain capacity shows an almost linear increase from 1.5% to approaching 5%. The strain increase of the 0.5% oiled composites over the strain capacity of the 0.3% oiled composites appears to have derived from the more than doubling of the number of multiple cracks (crack spacing reduced from 7.5 to 3.5 mm). This suggests that the 0.3% oiled composite may be in a transition from quasibrittle to

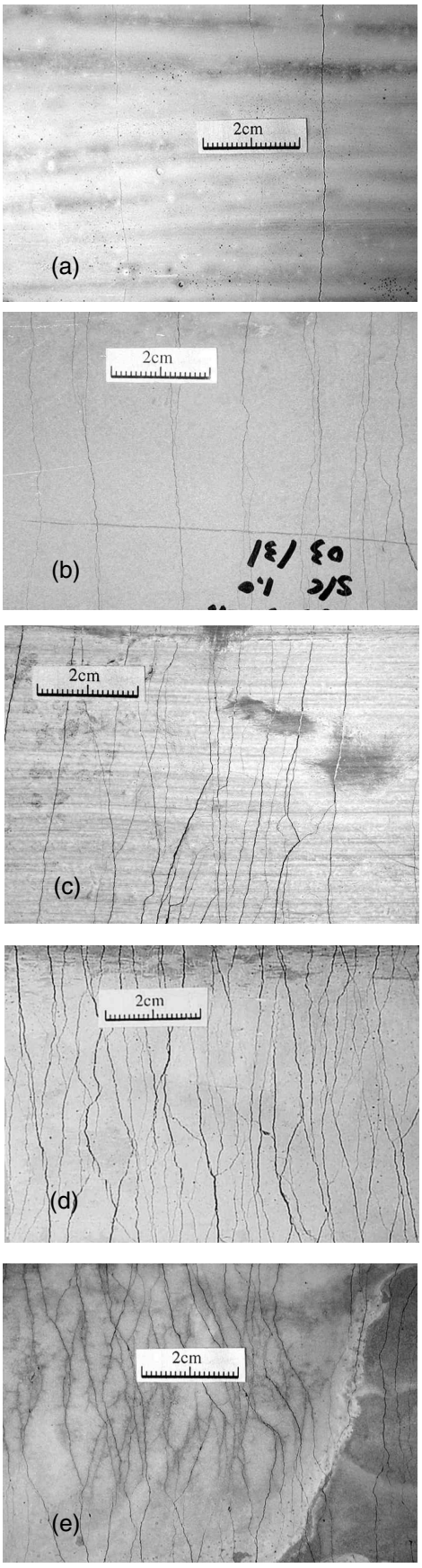


*Fig. 11—Effect of oiling agent content on multiple crack pattern of PVA-ECC: (a) 0% ($e_{cu}$ = 0.9%); (b) 0.3% ($e_{cu}$ = 1.9%); (c) 0.5% ($e_{cu}$ = 2.8%); (d) 0.8% ($e_{cu}$ = 3.6%); and (e) 1.2% ($e_{cu}$ = 4.7%).*

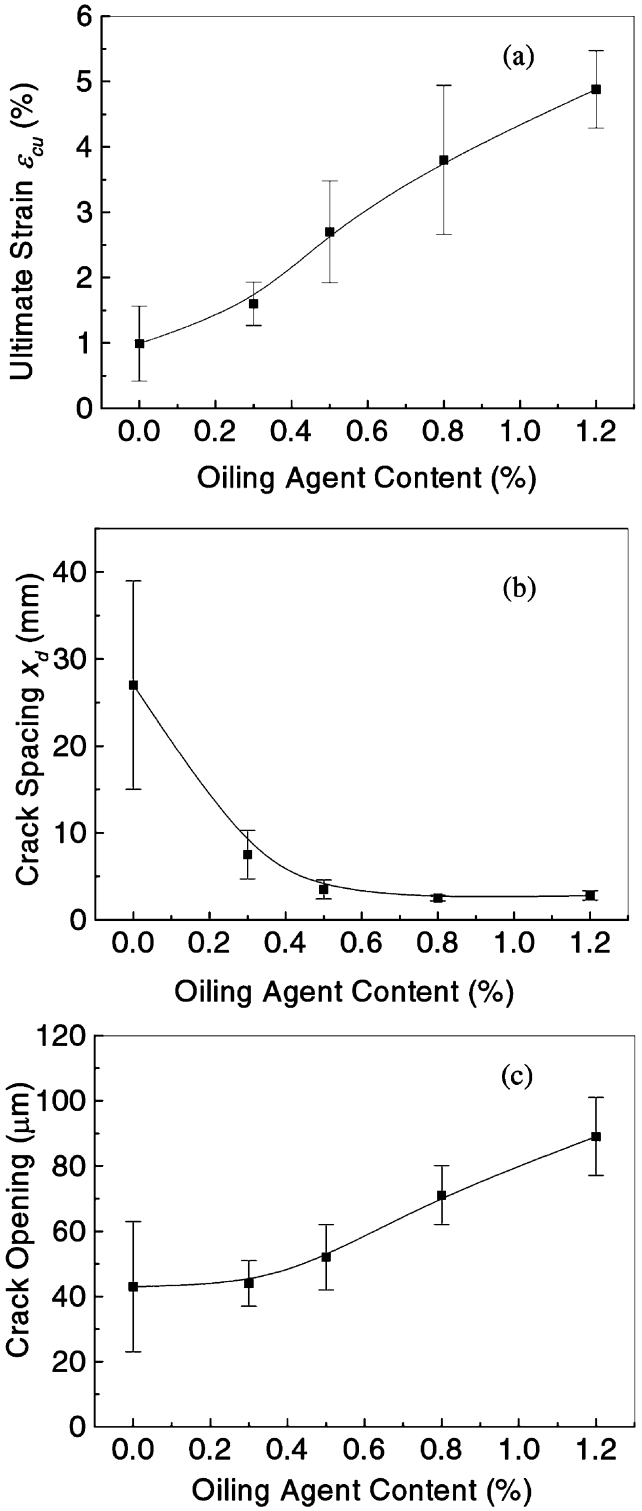


*Fig. 12—Influence of oiling content on: (a) tensile strain capacity; (b) crack spacing; and (c) crack opening.*

strain-hardening behavior, that is, the inequality in Eq. (2) is barely satisfied. In fact, the measure $J_{tip}$ for this matrix is between 4.5 to 7.2 J/m$^2$. In contrast, the further strain increase of the 0.8% oiled composites over the strain capacity of the 0.5% oiled composites appears to have derived mainly from the significantly enhanced crack opening (from 52 to 71 μm). The relatively smaller crack spacing reduction from 3.5 to 2.5 mm suggests that multiple crack saturation is being approached with the 0.8% oiling content, and this is further

confirmed by no further reduction in crack spacing of the 1.2% oiled composites. In Reference 25, Kanda and Li proposed that to achieve saturated strain-hardening cracking, the index $J_b'/J_{tip}$ should be larger than 3 to account for the material constituent variations along the length of the specimen. Although this criterion was established on the experimental observation from the polyethylene ECC composites, it is also consistent with the findings in this study. As shown in Table 3, the index $J_b'/J_{tip}$ increases with higher oiling content and reaches 3 at about 0.8%, which is also the transition point of cracking saturation.

The properties trends for the composites (Fig. 12) are consistent with those for the fiber/matrix interface as presented in Fig. 7. As the oiling content increases, the interface properties drop, allowing the fibers to slip out with less damage and rupture, and enhancing the bridging properties and composite tensile strain capacity. Furthermore, the prediction of optimal chemical bond $G_d$ less than 2.2 J/m$^2$ and frictional bond $\tau_0$ of 1.0 to 2.0 MPa by Wu[17] for $J_b'$ high enough for saturated multiple cracking appears to be born out by these experiments. Specifically, the experimental results on interface properties in Fig. 7 suggest that the oiling content should be at least 0.8% to achieve the desired $G_d$ and $\tau_0$. The experimental results on composite properties in Fig. 11 and 12 confirm that the 1.2% oiled composite possesses the highest tensile strain capacity with the best multiple-crack saturation while the 0.8% oiled composite already shows satisfying strain-hardening and multiple cracking behavior.

The correlation between composite test results and single-fiber test results can be further studied by examining the length of protruding fibers from a fracture surface of the composite by completely separating two halves of a specimen. Figure 13 confirms the expectation that more and longer embedded fibers can be pulled out in the increasingly higher oiled composite. For example, the highly oiled (1.2%) composite shows a protruded fiber length averaging approximately 2 mm, while the non-oiled composite shows the majority of protruded fiber lengths below 1 mm, indicating a heavier degree of fiber rupture. This means that in the highly oiled composites fewer fibers are damaged by the delamination process depicted in Fig. 8 and 9. However, it should be pointed out that for complete pullout, the protruded fiber lengths should vary between 0 and 6 mm, with an average of 3 mm for random fiber orientation because the fiber length is 12 mm. Hence, even for the 1.2% oiled fiber, some amount of these fibers are likely rupturing in the composite, most likely during the slip-hardening stage.

By reducing the interface properties $G_d$, $\tau_0$, and $\beta$, the higher oiling content also reduces the bridging stiffness or the slope of the $\sigma(\delta)$ curve of the resulting composites. This implies that for a given load level during composite strain-hardening, it may be expected to experience the larger crack opening $\delta$. This is consistent with the experimentally monitored crack width (Fig. 12(c)).

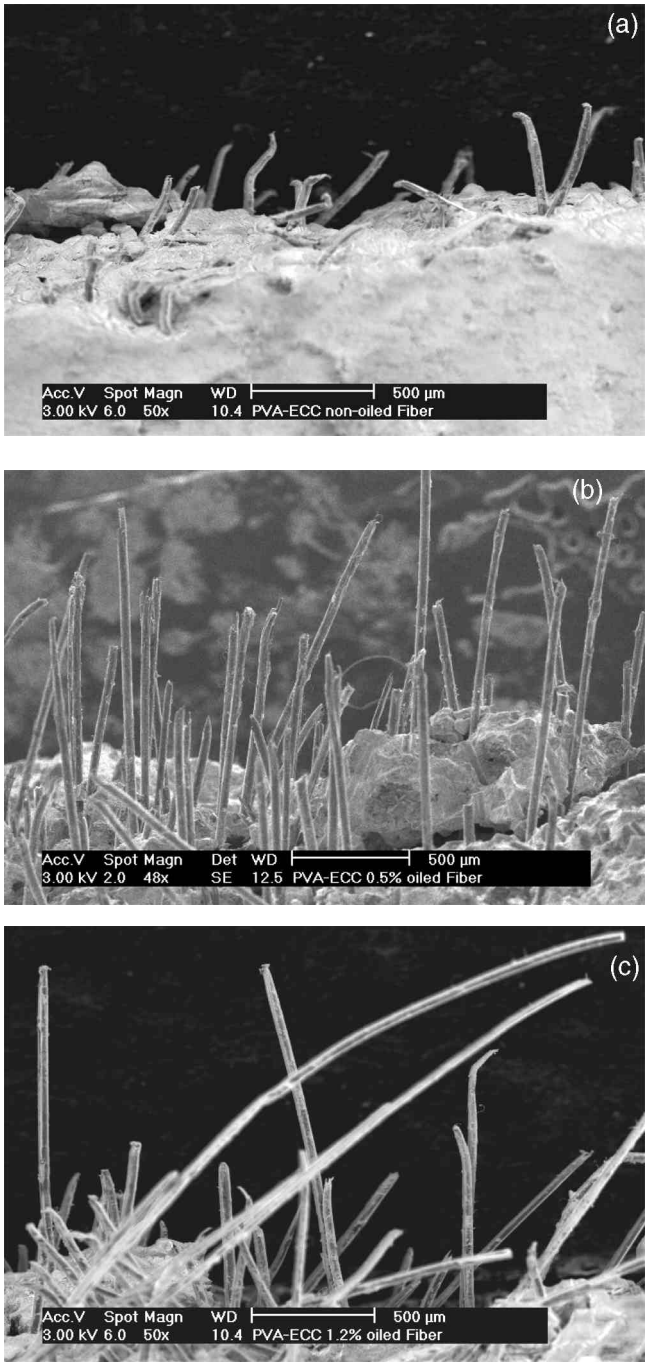


*Fig. 13—Micrographs showing protruded fibers on fracture surfaces of PVA-ECC specimens with: (a) 0%; (b) 0.5%; and (c) 1.2% oiling.*

## CONCLUSIONS AND FURTHER DISCUSSIONS

The following conclusions can be drawn:

1. Unlike many common fiber/matrix composite systems, the bonding between PVA fiber and a cementitious matrix is too high and needs to be lowered. The oiling agent is demonstrated via a single-fiber pullout test to be effective in counteracting the excessive chemical bond and slip-hardening effect for PVA fibers in cementitious composites;

2. Tensile strain-hardening with strain capacity in excess of 4% can be achieved with PVA fiber-reinforced ECC composites provided that the interface is properly tailored to control the magnitudes of $G_d$, $\tau_0$, and $\beta$. The oiling content of 1.2% gives the best result in this series of tests; and

3. A micromechanical model of tensile strain-hardening in cementitious composites provides useful guidance for microstructure tailoring. In this experimental study, the effective guidance for interface property tailoring for high $J_b'$ is revealing.

While this paper focuses on tailoring of the fiber/matrix interface for strain-hardening in PVA-ECC, it is important to point out that a holistic approach is necessary for truly optimal composite design. Tailoring of the fiber, matrix, and fiber/

matrix interface should be carried out in an integrative scheme, as attempted by Wu.[17] As an example, Li, Wang, and Wu. demonstrated that the optimal amount of sand in the matrix varies with the oiling content of the fiber due to the matrix fracture toughness and pre-existing flaw distribution.[18] This emphasizes the importance of treating ECC as a composite system in which the three phases interact with one another. The modification of one phase may necessitate the adjustments of the other phases for truly optimal composite performance.

Furthermore, it may be expected that the optimal oiling content could be different for composites manufactured with different processing routes. For example, if an extrusion method is applied,[15,26] the microstructure of the interphasal zone can be denser than that in composites formed by a normal casting technique. For such composites, the oiling content needed is likely higher to compensate for the increased bond induced by the stronger compaction process.

Finally, it should be pointed out that the use of oiling is only one means of tailoring the fiber/matrix interface. Recent research in PVA-reinforced cementitious composites suggests that the presence of fly ash in the matrix can influence the interfacial behavior.[19,27] Further investigations in the combined use of oiling and fly ash are needed for continued enhancement of composite performance.

## ACKNOWLEDGMENTS

Supports by Kuraray Co., Ltd. (Osaka, Japan) and NSF Grand No. CMS-0070035 (Program Director J. Scalzi) are gratefully acknowledged. The authors would like to thank US Silica, Co. for providing the fine sand; Lafarge Corp. for supplying the portland cement; and the Dow Chemical Co. for supplying the chemical additives used in this research program.

## REFERENCES

1. Cotterell, B., and Mai, Y. W., *Fracture Mechanics of Cementitious Materials*, Chapman and Hall, 1996.

2. Aveston, J.; Cooper, G. A.; and Kelly, A., "Single and Multiple Fracture," *Proceedings of Properties of Fiber Composites*, National Physical Laboratory, IPC Science and Technology Press, Guildford, UK, 1971, pp. 15-24.

3. Li, V. C., and Leung, C. K. Y., "Steady State and Multiple Cracking of Short Random Fiber Composites," *ASCE Journal of Engineering Mechanics*, V. 188, No. 11, 1992, pp. 2246-2264.

4. Li, V. C., and Wu, H. C., "Conditions for Pseudo Strain-Hardening in Fiber Reinforced Brittle Matrix Composites," *Journal Applied Mechanics Review*, V. 45, No. 8, Aug. 1992, pp. 390-398.

5. Naaman, A. E., and Homrich, J. R., "Tensile Stress Strain Properties of SIFCON," *ACI Materials Journal*, V. 86, No. 3, May-June 1989, pp. 244-251.

6. Bouygues; Lafarge; and Rhodia Chimie, "Concrete Comprising Organic Fibers Dispersed in a Cement Matrix, Concrete Cement Matrix and Premixes," *French Patent PCT/FR99/01145*, May 12, 1999.

7. Li, V. C., "Engineered Cementitious Composites—Tailored Composites Through Micromechanical Modeling," *Fiber Reinforced Concrete: Present and the Future*, N. Banthia, A. Bentur, and A. Mufti, eds., Canadian Society for Civil Engineering, Montreal, 1998, pp. 64-97.

8. Li, V. C., and Hashida, T., "Engineering Ductile Fracture in Brittle Matrix Composites," *Journal of Materials Science Letters*, V. 12, 1993, pp. 898-901.

9. Maalej, M.; Li, V. C.; and Hashida, T., "Effect of Fiber Rupture on Tensile Properties of Short Fiber Composites," *ASCE Journal of Engineering Mechanics*, V. 121, No. 8, 1995, pp. 903-913.

10. Li, V. C., "Damage Tolerance of Engineered Cementitious Composites," *Advances in Fracture Research*, Proceedings, 9th ICF Conference on Fracture, Sydney, Australia, B. L. Karihaloo; Y. W. Mai; M. I. Ripley; and R. O. Ritchie, eds., Pub. Pergamon, UK, 1997, pp. 619-630.

11. Maalej, M., and Li, V. C., "Introduction of Strain Hardening Engineered Cementitious Composites in the Design of Reinforced Concrete Flexural Members for Improved Durability," *ACI Structural Journal*, V. 92, No. 2, Mar.-Apr. 1995, pp. 167-176.

12. Fischer, G., and Li, V. C., "Structural Composites with ECC," *The 6th ASCCS International Conference: Steel-Concrete Composite Structures*, Los Angeles, Calif., Mar. 2000, pp. 1001-1009.

13. Parra-Montesinos, G., and Wight, J. K., "Seismic Response of Exterior RC Column-to-Steel Beam Connections," *ASCE Journal of Structural Engineering*, V. 126, No. 10, Oct. 2000, pp. 1113-1121.

14. Fukuyama, H.; Sato, Y.; Li, V. C.; Matsuzaki, Y.; and Mihashi, H., "Ductile Engineered Cementitious Composite Elements for Seismic Structural Applications," *Proceedings of the 12th World Conference of Earthquake Engineering,* 2000, No. 1672.

15. Shao, Y., and Shah, S. P., "Mechanical Properties of PVA Fiber Reinforced Cement Composites Fabricated by Extrusion Processing," *ACI Materials Journal*, V. 94, No. 6, Nov.-Dec. 1997, pp. 555-564.

16. Kanda, T., and Li, V. C., "Interface Property and Apparent Strength of a High Strength Hydrophilic Fiber in Cement Matrix," *ASCE Journal of Materials in Civil Engineering*, V. 10, No. 1, 1998, pp. 5-13.

17. Wu, C., "Micromechanical Tailoring of PVA-ECC for Structural Applications," PhD thesis, Department of Civil and Environmental Engineering, University of Michigan, Ann Arbor, Mich., Jan., 2001.

18. Li, V. C.; Wang, S.; and Wu, C., "Tensile Strain-Hardening Behavior of PVA-ECC," *ACI Materials Journals*, V. 98, No. 6, Nov.-Dec. 2001, pp. 483-492.

19. Redon, C.; Li, V. C.; Wu, C.; Hoshiro, H.; Saito, T.; and Ogawa, A., "Measuring and Modifying Interface Properties of PVA Fibers in ECC Matrix," *ASCE Journal of Materials in Civil Engineering*, V. 13, No. 6, Nov.-Dec., 2001, pp. 399-406.

20. Marshall, D., and Cox, B. N., "A J-Integral Method for Calculating Steady-State Matrix Cracking Stress in Composites," *Mechanics of Materials*, V. 7, No. 8, 1988, pp. 127-133.

21. Li, V. C., "Post-Crack Scaling Relations for Fiber-Reinforced Cementitious Composites," *ASCE Journal of Materials in Civil Engineering*, V. 4, No. 1, 1992, pp. 41-57.

22. Lin, Z.; Kanda, T.; and Li, V. C., "On Interface Property Characterization and Performance of Fiber Reinforced Cementitious Composites," *Journal of Concrete Science and Engineering*, RILEM, V. 1, 1999, pp. 173-184.

23. Katz, A., and Li, V. C., "A Special Technique for Determining the Bond Strength of Carbon Fibers in Cement Matrix by Pullout Test," *Journal of Materials Science Letters*, V. 15, 1996, pp. 1821-1823.

24. Zhang, J.; Li, V. C.; Nowak, A.; and Wang, S., "Introducing Ductile Strip for Durability Enhancement of Concrete Slabs," *ASCE Journal of Materials in Civil Engineering*, V. 14, No. 3, June 2002, pp. 253-261.

25. Kanda, T., and Li, V. C., "Multiple Cracking Sequence and Saturation in Fiber Reinforced Cementitious Composites," *Concrete Research and Technology*, JCI, V. 9, No. 2, 1998, pp. 19-33.

26. Stang, H., and Li, V. C., "Extrusion of ECC-Material," *Proceedings of High Performance Fiber Reinforced Cement Composites 3 (HPFRCC 3)*, H. Reinhardt and A. Naaman, eds., Chapman & Hull, 1999, pp. 203-212.

27. Peled, A.; Cyr, M. F.; and Shah, S. P., "High Content of Fly Ash (Class F) in Extruded Cementitious Composites," *ACI Material Journal*, V. 97, No. 5, Sept.-Oct. 2000, pp. 509-517.